

Synchronization Sensitivity of Enhanced CDMA Array-Receivers to Fast Channel Time-Variations and to Shaping-Pulse Design*

Karim CHEIKHROUHOU
École Nationale d'Ingénieurs de Tunis
BP 37, Le Belvédère
Tunis, 1002, Tunisia
cheikhro@inrs-telecom.quebec.ca

Sofiene AFFES and Paul MERMELSTEIN
INRS-Télécommunications, Université du Québec
900, de la Gauchetière Ouest, Niveau C, CP 644
Montreal, Quebec, H5A 1C6, Canada
{affes,mermel}@inrs-telecom.quebec.ca

Abstract

We previously reported on the severe impact synchronization errors may have on the spectrum efficiency of wideband CDMA networks and on the significant performance gains of STAR over the 2D-RAKE at similar order in complexity. Here we further enhance the 2D-RAKE performance by incorporating a high-resolution early-late gate with a clamping state and further reduce the complexity of STAR. New complexity and performance assessments indicate that STAR at a comparable computational load, increases its performance advantage over the enhanced 2D-RAKE in the presence of fast channel time-variations even with pulse distortions or at different rolloff factors.

1. Introduction

Wideband CDMA for third generation systems requires significant enhancement in receiver operation, *e.g.*, signal combining, power control or channel coding, to lead to a high spectrum efficiency and an increase in cell capacity. However, such high-capacity operation requires synchronization at significantly reduced SNR levels.

Synchronization with the conventional RAKE, which relies on the early-late gate [14], may seriously limit the SNR tolerable. Previous works assessing capacity assuming perfect synchronization may provide over optimistic results. We study the impact of practical synchronization requirements on two space-time array-processors, namely the 2D-RAKE [12],[9] and STAR [6],[7].

Previously [6] we integrated the early-late gate component into the 2D-RAKE in a new structure that exploits the processing capabilities of antenna-arrays. In this contribution, we improve its performance by adding [6] a high-

resolution feature [7] to the early-late gate. In [6] we proposed significant enhancements to STAR [5]. Here we further improve its complexity by carrying out space-time combining before despreading [3]. We thereby restrict the number of costly despreading steps to the less frequent channel update operations. The complexity of the despreading steps is further reduced by replacing time convolutions by fast FFT-based convolutions. New complexity and performance assessments indicate that STAR at a comparable computational load, increases its performance advantage over the enhanced 2D-RAKE in the presence of fast channel time-variations even with pulse distortions or at different rolloff factors.

2 Data Model

We consider a single-user receiver structure on the uplink direction (portable-to-base station) of a cellular CDMA system. Let us assume that each base station is equipped with M receiving antennas. We consider P propagation paths in a selective fading multipath environment where the time-delay spread $\Delta\tau$ is small compared to T . The user PSK symbol sequence, binary or quaternary, is first differentially encoded at a rate $1/T$, where T is the bit duration. The resulting sequence $b(t)$ is then spread with a long PN code $c(t)$ at a rate $1/T_c$ where T_c is the chip pulse duration. The processing gain is given by $L = T/T_c$.

A preprocessing unit in STAR (see Fig. 1) passes the above observation vector $X(t)$ through a matched-pulse filter and provides the matched-filtering observation vector for frame number n over the time-interval $[0, 2T - T_c]$ in successive overlapping frames of period T by:

$$Y_n(t) = \frac{1}{T_c} \int_{D_\phi} X(nT + t + t') \phi(t') dt', \quad (1)$$

where D_ϕ denotes the temporal support¹ of the shaping

¹For a rectangular pulse, D_ϕ is $[0, T_c]$. In practice and as assumed

*Work supported by the Bell/Nortel/NSERC Industrial Research Chair in Personal Communications and by the NSERC Research Grants Program.

pulse $\phi(t)$ [5]. After sampling at the chip rate and framing over $2L - 1$ chip samples at the bit rate by the pre-processing unit (see Fig. 1), we obtain the $M \times (2L - 1)$ matched-filtering observation matrix:

$$\begin{aligned} \mathbf{Y}_n &= \sum_{k=-1}^{+1} \psi_n b_{n+k} \mathbf{Y}_{k,n} + \mathbf{N}_n = s_n \mathbf{Y}_{0,n} + \mathbf{I}_{\text{ISI},n} + \mathbf{N}_n \\ &\simeq s_n \mathbf{Y}_{0,n} + \mathbf{N}_n, \end{aligned} \quad (2)$$

where $s_n = \psi_n b_n = \psi(nT)b(nT)$ is the signal component, b_n is the transmitted DBPSK or DQPSK data sequence and ψ_n^2 is the total received power. For $k = -1, 0, +1$, $\mathbf{Y}_{k,n}$ is the channel response $H(t)$, first convolved by the code segment that spreads b_{n+k} , matched-filtered, then sampled at the chip-rate. For simplicity, the system model of Eq. (2) does not identify explicitly the ISI (inter-symbol interference) matrix $\mathbf{I}_{\text{ISI},n}$ which represents the interference from adjacent symbols b_{n-1} and b_{n+1} but dumps it into the noise.

After despreading the matched-filtering observation matrix \mathbf{Y}_n of Eq. (2), we obtain the $M \times L$ -dimensional post-correlation observation matrix \mathbf{Z}_n of the post-correlation model (PCM) as follows [5]:

$$\mathbf{Z}_n = s_n \mathbf{H}_n + \mathbf{N}_{\text{PCM},n} = b_n \psi_n \mathbf{G}_n \mathbf{\Upsilon}_n \mathbf{D}_n^T + \mathbf{N}_{\text{PCM},n}, \quad (3)$$

where $\mathbf{H}_n = \mathbf{G}_n \mathbf{\Upsilon}_n \mathbf{D}_n^T$ with norm fixed to \sqrt{M} is the $M \times L$ spatio-temporal propagation matrix which yields $\mathbf{Y}_{0,n}$ after spreading $H(t)$ with the code segment of b_n , and $\mathbf{J}_n = \mathbf{G}_n \mathbf{\Upsilon}_n$ is the spatial response matrix which includes the effects of path loss, Rayleigh fading and shadowing. \mathbf{G}_n is the $M \times P$ propagation matrix, and $\mathbf{\Upsilon}_n = \text{diag}[\varepsilon_{1,n}, \dots, \varepsilon_{P,n}]$ is the $P \times P$ diagonal matrix of normalized power ratios over multipaths $\varepsilon_{p,n}^2$ (i.e., $\sum_{p=1}^P \varepsilon_{p,n}^2 = 1$). $\mathbf{D}_n = [D_{1,n}, \dots, D_{P,n}]$ is the $L \times P$ -dimensional time-response matrix with columns:

$$D_{p,n} = [\rho_c(-\tau_{p,n}), \rho_c(T_c - \tau_{p,n}), \dots, \rho_c((L-1)T_c - \tau_p)]^T,$$

where $\{\tau_{p,n}\}_{p=1,\dots,P} \in [0, T)$ are the time-varying multipath-delays along the P paths and $\rho_c(t)$ is a truncated raised-cosine pulse which corresponds to the correlation function of a square-root raised-cosine shaping-pulse $\phi(t)$. $\mathbf{N}_{\text{PCM},n}$ is the $M \times L$ -dimensional spatio-temporal uncorrelated noise matrix after despreading with variance σ_N^2 .

3 New Receiver Enhancements

3.1 Enhanced 2D-RAKE

To further enhance the performance of the 2D-RAKE proposed in [6], we replace the energy-based early-late decision rule there (see Eq. (5) in [6]) by the following in this paper, it is the temporal support of a truncated square-root raised-cosine.

eigenvalue-based alternative rule [7]:

$$a_{p,n} = \text{Sign} \left\{ \hat{\lambda}_n^+(p) - \hat{\lambda}_n^-(p) \right\}, \quad (4)$$

where $\{\hat{V}_n^+(p), \hat{\lambda}_n^+(p)\}$ and $\{\hat{V}_n^-(p), \hat{\lambda}_n^-(p)\}$ denote the pairs of eigenvector-eigenvalue estimates of the early and late sample matrices $\hat{R}_{ZZ,n}^+(p)$ and $\hat{R}_{ZZ,n}^-(p)$ of the p -th finger, respectively. The new rule adds a ‘‘high-resolution’’ feature (i.e., based on signal subspace characterization) to the tracking step, well known for its increased robustness to noise.

To improve the tracking performance and reduce timing errors, early-late loops may include an additional ‘‘clamped’’ state whereby the estimated time-delay is kept constant if the corresponding gap between the early-late measurements is below a given threshold. We incorporate this approach into the above eigenvalue-based loop as follows [7]:

$$a_{p,n} = \begin{cases} \text{Sign} \{ \lambda_n^+(p) - \lambda_n^-(p) \} \\ \quad \text{if } |\lambda_n^+(p) - \lambda_n^-(p)| > \lambda_{\text{TH}}, \\ 0 \text{ otherwise,} \end{cases} \quad (5)$$

$$\hat{\tau}_{p,n+1} = \hat{\tau}_{p,n} + a_{p,n} T_{sc}, \quad (6)$$

$$\hat{G}_{p,n+1} = \begin{cases} \hat{V}_n^+(p) \text{ if } a_{p,n} = +1, \\ \hat{V}_n^-(p) \text{ if } a_{p,n} = -1, \\ \hat{V}_n^0(p) \text{ if } a_{p,n} = 0, \end{cases} \quad (7)$$

where λ_{TH} is the ‘‘clamping’’ threshold² over the gap between the early-late eigenvalues below which the time-delay estimate is not incremented. The new 2D-RAKE early-late loop requires that we further compute the sample matrix $\hat{R}_{ZZ,n}^0(p)$ of $Z_{p,n}^0 = Z_n(\hat{\tau}_{p,n})$ and its principal eigenvector $\hat{V}_n^0(p)$. Used later as a reference for performance comparisons, this enhanced version shall offer up to 30% gain in capacity over the one previously suggested [6] when combined with the 2D-RAKE.

3.2 Enhanced STAR

In [6], we significantly reduced complexity by introducing minimum channel update where channel identification is updated every n_{ID} symbols. From one update to another, note that only despreading and combining operations are active. One way to further reduce complexity dramatically is to further freeze the very expensive dspsreading operation when keeping the channel estimate on hold while carrying out spatio-temporal combining over the data before despreading (see Fig. 1-b). We hence introduce the matched-filtering observation matrix after $M(2L - 1) \times 1$ -dimensional vector reshaping as follows [3],[4] (see Fig. 1-b):

$$\underline{\mathbf{Y}}_n \simeq s_n \underline{\mathbf{Y}}_{0,n} + \underline{\mathbf{N}}_n, \quad (8)$$

²Note that the tracking response to fast time-delay drifts speeds up with larger thresholds while tracking errors decrease with smaller ones.

which after despreading, provides the $ML \times 1$ -dimensional post-correlation vector Z_n (see [6],[7],[3],[4] and Fig. 1-a). In the equation above, $\hat{Y}_{0,n}$ is the spread channel version of \hat{H}_n . Hence, the MRC combining operation [6] becomes [7] (see Fig. 1-b):

$$\hat{s}_n = \text{Real} \left\{ \mathbf{W}_n^H \mathbf{Y}_n \right\} = \text{Real} \left\{ \frac{\hat{Y}_{0,n}^H \mathbf{Y}_n}{\|\hat{Y}_{0,n}\|^2} \right\}. \quad (9)$$

Note that the dimension of both $\hat{Y}_{0,n}$ and \mathbf{Y}_n is adequately truncated to $M(L + L_{\Delta} - 1) \times 1$ when further saving complexity using a reduced processing window of length L_{Δ} [6],[7].

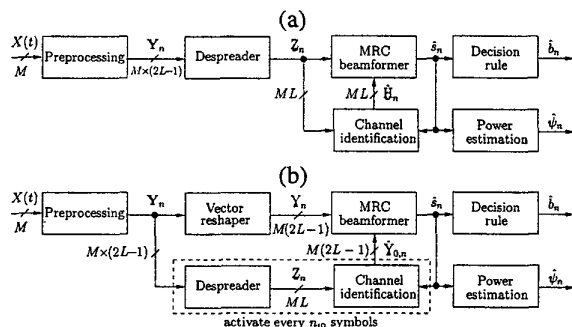


Figure 1. Block diagram of STAR receiver with MRC implemented (a): after despreading, (b): before despreading.

Note also that the reconstruction of $\hat{Y}_{0,n}$ for combining needs a respreading operation of \hat{H}_n at each iteration when using long spreading codes. When using short codes, it becomes redundant after covering one code cycle and even unnecessary when the code period is equal to the symbol duration. Complexity is thereby even more reduced. For the complexity assessment coming next, we define n_{CR} , the number of symbol iterations required before channel respreading and reconstruction of $\hat{Y}_{0,n}$. It is set to 1 for long codes and to n_{ID} for short codes with length L .

In [6], we implemented despreading with computationally more expensive time convolutions. Here, all despreading (and respreading) operations are implemented using the OLA (overlap-add) FFT/IFFT-based fast convolution technique [11], hence the significantly reduced complexity orders in \log_2 and the difference in complexity assessment from [6] (see next).

4 New Complexity Assessment

We plot in Fig. 2 the complexity required per user in Mops for STAR and the 2D-RAKE versus the processing

gain L in 4.096 Mcps bandwidth with $M = 2$ antennas and $P = 3$ multipaths. Complexity of the 2D-RAKE takes into account multipath tracking by the early-late gate using Eqs. (5)-(7), as well as multipath reacquisition over a sample-matrix smoothing duration of $n_{SD} = 200$ symbols once every n_{RA} symbols (*i.e.*, reacquisition period) using Eqs. (2)-(4) in [6].

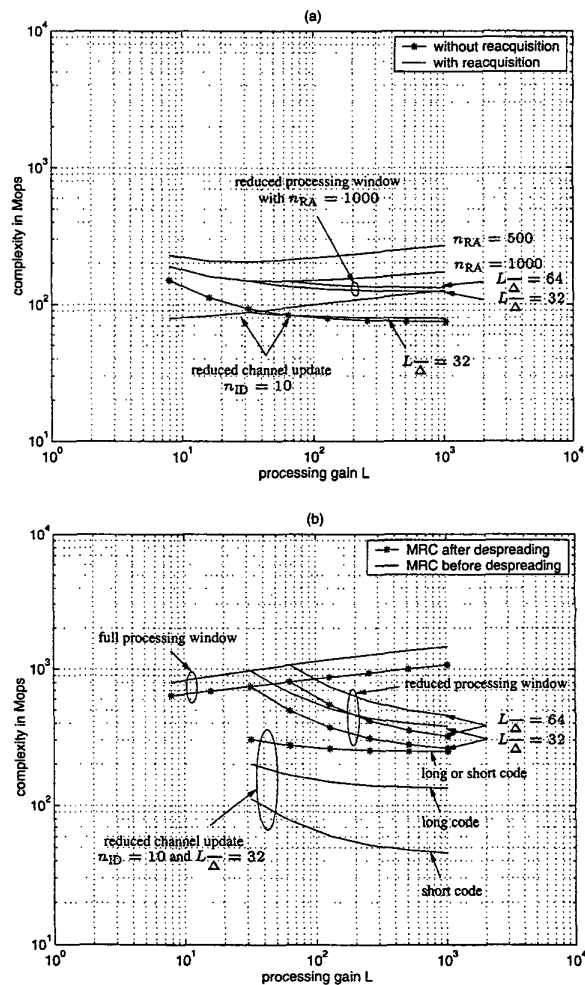


Figure 2. Estimated complexity vs. the processing gain L in 4.096 Mcps for $M = 2$ antennas and $P = 3$ multipaths. (a): 2D-RAKE. (b): STAR.

Figure 2 shows that implementation of STAR over a reduced processing window, still best suited to large processing gains [6], lowers complexity more dramatically at lower data rates. Whatever is the size of the processing window, MRC after despreading requires less complexity than MRC before despreading with full channel update (no longer true

	$f_D = 106 \text{ Hz}, \frac{d\tau}{dt} = 4 \text{ ppm}$			
	2D-RAKE		STAR	
	Ideal Sync.	Active Sync.	Ideal Sync.	Active Sync.
	9.6 Kbps (DBPSK) @ 10^{-3}			
SNR_{req} (dB)	1.1	1.5	-2.3	-1.6
C (users/cell)	179	163	424	348
ζ (bps/Hz/antenna)	0.039	0.036	0.093	0.077
	128 Kbps (DQPSK) @ 10^{-5}			
SNR_{req} (dB)	2.8	6.1	2.1	2.3
C (users/cell)	4	2	5	4
ζ (bps/Hz/antenna)	0.031	0.016	0.039	0.031

Table 1. Impact of synchronization on performance of both the 2D-RAKE and STAR at fast Doppler and multipath delay-drifts.

with multi-user STAR [3]). Minimum channel identification update on the other hand, still best suited to high data-rates [6], reduces complexity significantly for lower processing gains and favors implementation of MRC before despreading, more so when using a short code (see impact of code length on performance in [10]). The 2D-RAKE similarly benefits from a reduced processing window and a minimum channel update in complexity reduction.

Overall, both complexity gains combined put STAR in the same computational order as the 2D-RAKE (or even below, see Fig. 2). As one example, for a processing gain of 32 and $n_{ID} = 10$, STAR would require about 110 Mops with a short code and about 200 Mops with a long code against 90 Mops per user for the 2D-RAKE. Processors offer today a computational power of about 10 Gops and render STAR very attractive both in complexity and performance (see next).

5 New Sensitivity Study and Conclusions

Details about the simulation setup can be found in [6],[7]. The following assessments use $M = 4$ antennas.

5.1 Impact of Fast Channel Time-Variations

We measure the impact of synchronization on the 2D-RAKE and STAR in the presence of fast channel parameter variations. We previously made this assessment with a slow Doppler shift f_D of about 2 Hz and a multipath delay-drift $\frac{d\tau}{dt}$ of 0.046 ppm [6]. Here, we increase f_D to about 106 Hz and $\frac{d\tau}{dt}$ up to 4 ppm, far beyond the 0.05 and 0.1 ppm uplink/downlink clock imprecision thresholds specified in the standards [1],[2].

Performance results shown in Tab. 1 suggest the following:

- Timing impact may become negligible in the presence of high Doppler even in the presence of very fast time-delay drifts. In this situation, channel identification errors stand out as the dominant factor in performance degradation compared to the sole effect of timing errors, more so at lower data rates. In the voice-rate case, the 2D-RAKE and STAR with perfect timing incur about 50 and 20% loss in spectrum efficiency, respectively, due to the Doppler increase by a factor 50 (see results in [6],[7]). Activation of timing with a delay drift 90 times faster adds just about 10 and 20% loss, respectively. In the high-rate case where channel variations are relatively slower, the additional impact of timing errors become far more significant, more so with the 2D-RAKE. Activation of synchronization incurs almost 50 and 20% loss in spectrum efficiency to the 2D-RAKE and STAR, respectively.

- Overall, STAR increases its performance advantage over the 2D-RAKE in the presence of faster channel parameter variations. We measure spectrum efficiency gains of about 110 and 100% for the voice and data rates, respectively, against the approximate 70 and 80% gains reported previously in the case of slow channel parameter variations (see results in [6],[7]).

The reduced channel update every n_{ID} symbols [6],[7] increases channel parameter variations (*i.e.*, n_{ID} times faster) and translates into performance losses. However, it reduces complexity significantly. We summarize below the resulting tradeoff between the complexity gain and the spectrum efficiency loss for both cases of slow and fast channel parameter variations using $n_{ID} = 10$.

With the channel update rate reduced by a factor 10, the 2D-RAKE and STAR gain about 40 and 55% in complexity in the voice-rate case and about 40 and 75% in the data-rate case, respectively (see Fig. 2). However, both the Doppler and the multipath delay-drifts become 10 times faster, relatively. In the slow channel case, increased channel variations from reduced update are not fast enough yet to result in noticeable degradation in performance [6],[7]. We measure about 0% loss in spectrum efficiency for both data rates. The reduced channel update option is extremely useful in this case.

In the fast channel case however, the 2D-RAKE and STAR incur 50 and 25% loss in spectrum efficiency in the data-rate case, at 0.008 and 0.023 bps/Hz/antenna, respectively. In the voice-rate case, channel variations become extremely fast and performance losses become unacceptable for both the 2D-RAKE and STAR. The reduced channel update option may still be useful in the most interesting high data-rate case to future wideband CDMA networks. However, if the trade of 25% performance loss for 75% complexity gain is acceptable with STAR, a trade of 50% per-

formance loss for 40% complexity gain is not with the 2D-RAKE. Even then, STAR with $n_{ID} = 10$ will outperform the 2D-RAKE with $n_{ID} = 1$ by about 50% in spectrum efficiency while requiring almost the same complexity cost.

5.2 Impact of Chip-Pulse Distortion

Simulation results above demonstrate that STAR outperforms the 2D-RAKE in spectrum efficiency due to enhancements in both combining and synchronization. Improvement in combining is clearly attributed to the fact that quasi-coherent demodulation and differential decoding of STAR perform better than differential demodulation of the 2D-RAKE. On the other hand, enhancement in synchronization suggests a new interpretation that the pulse matching approach of STAR is superior in performance to the finger extraction principle of the 2D-RAKE.

One concern that arises in this case is whether STAR is more sensitive to waveform distortions than the 2D-RAKE since it matches the nominal chip-pulse waveform, an essential assumption to the tracking and combining steps in STAR. The answer will determine whether STAR could maintain its performance advantage over the 2D-RAKE in more practical operating conditions. Standard proposals indeed tolerate an amount of waveform distortions [1],[2]. In a third set of simulations, we hence assess the impact of chip-pulse distortions over capacity and spectrum efficiency.

We define³ the pulse distortion in percent as the square root of the energy of the pulse waveform error over the energy of the pulse waveform itself. For a given distortion ratio, we generate $N_c + 1$ i.i.d. random Gaussian noise samples with the appropriate energy and add them to the nominal pulse waveform samples in the received signals ($N_c + 1$ is the number of shaping-pulse coefficients). Errors are independent from one symbol to another.

In Fig. 3, we plot the capacity and spectrum efficiency performance in the voice-rate case for both the 2D-RAKE and STAR versus the pulse distortion amount in %.

Curves suggest the following:

- Capacity and *a fortiori* spectrum efficiency decrease almost linearly with the distortion energy, a signal leakage processed as interference to the receiver.
- Standards [1],[2] suggest maximum distortion thresholds of 12.5 and 17.5% on the uplink and downlink, respectively. Performance degradation due to a pulse distortion of 15% is weak and less than 5% for both the 2D-RAKE and STAR.
- Even if STAR matches the nominal waveform while the 2D-RAKE extracts fingers (*i.e.*, pulse peaks), pulse distortions relatively impact the performance of both receivers in the same way. This suggests that STAR maintains its performance advantage over the 2D-RAKE due to enhanced

³This definition is similar to that suggested by recent 3G standard proposals [1],[2].

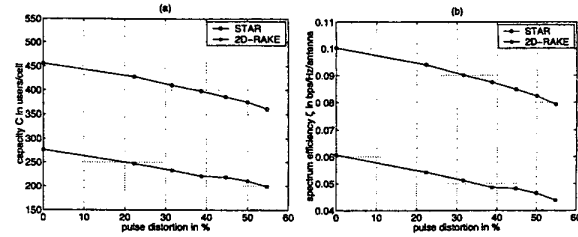


Figure 3. Impact of pulse distortion on (a): capacity, (b): spectrum efficiency at 9.6 Kbps.

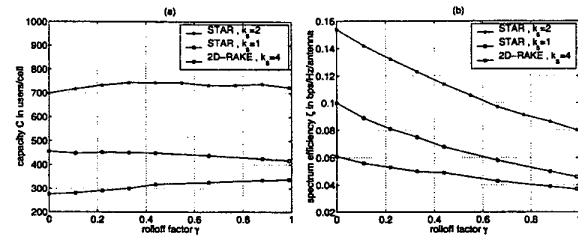


Figure 4. Impact of rolloff factor γ on (a): capacity, (b): spectrum efficiency at 9.6 Kbps.

synchronization, even in the presence of pulse waveform distortions. sample result in the same distortion ratio on average.

5.3 Impact of Rolloff Selection and Oversampling

Another concern that may question the established performance advantage of STAR over the 2D-RAKE is the rolloff factor selection. For illustration purposes and for simplicity, timing gains have been demonstrated with a sinc function (*i.e.*, rolloff 0) [6],[7]. For practical design purposes though, systems would implement raise-cosine filters with a rolloff factor higher than 0 to avoid sharp spectral decays. Standard proposals suggest a rolloff factor of 0.22 [1],[2]. STAR would then extract and match pulses sampled at a rate lower than their bandwidth.

The question that arises in this case is whether STAR would loose its performance advantage over the 2D-RAKE due to possible timing degradation from a sampling rate below the bandwidth. In a fourth set of simulations, we hence assess the impact of rolloff factor selection on performance (assuming a bandwidth higher than 5 MHz).

Capacity and spectrum efficiency results shown in Fig. 4 versus the rolloff factor in the voice-rate case suggest the following:

- As anticipated in [5], STAR without chip oversampling is extremely robust to the pulse waveform design (see [15],[8])

for specific work on waveform design and selection). By linear phase fitting in the frequency domain, it always extracts from the received chip waveform the closest sinc pulse in the tracking process [5]. It hence delivers about the same capacity performance even if the raised-cosine shaping pulse occupies a bandwidth higher than the chip-rate. Degradation due to frequency aliasing becomes noticeable only at rolloff factors close to 1, but it remains negligible.

- The 2D-RAKE, with an oversampling factor $k_s = 4$, reduces its sensitivity to timing errors and slightly increases its capacity performance at higher rolloff factors. Yet at a rolloff factor of 0.22 [1],[2], STAR advantage over the 2D-RAKE is still significant at about 55% in spectrum efficiency.

- On the light of the above observations, we investigated the impact of chip oversampling on STAR by a factor $k_s = 2$. Oversampling virtually doubles the processing gain at merely no increase in computational order (see Fig. 2) yet it introduces a “sampling diversity” gain that further underlines the strength of the pulse-matching approach of STAR versus finger extraction in RAKE-type receivers. Indeed, STAR capacity enhancement due to oversampling is very significant and increases from about 55% for $\gamma = 0$ to about 75% for $\gamma = 1$. The capacity increase at higher rolloffs indicates that oversampling above the chip-rate avoids aliasing (see above) as already shown in fractional sampling in equalization [13], and enables exploitation of increasing robustness to timing errors. At a rolloff of 0.22 [1],[2], the spectrum efficiency advantage of STAR with oversampling by factor 2 over the 2D-RAKE with oversampling by factor 4 is very high at about 150%.

5.4 Conclusions

Overall, it is worth noting that STAR avoids chip-oversampling and that its resolution is not limited by a fixed refining chip-fraction. It exploits the signal energy from the entire shaping pulse, not only its peak (*i.e.*, RAKE-finger), hence it generates better estimates for the delay of each path despite possible waveform distortions and better exploits chip oversampling. It identifies a stronger space-time channel vector instead of separate multipath channel vectors with weaker fractioned powers. Without a pilot, it achieves coherent detection and differential decoding instead of less efficient differential demodulation. Overall, STAR outperforms both the 2D-RAKE in space-time signal combining, and the early-late gate in synchronization. At practically the same order of complexity, performance gains are significant with one (*i.e.*, 1D-RAKE) or more antennas, for low or high data rates, for slow or fast channel variations.

References

- [1] 3rd Generation Partnership Project (3GPP), Technical Specification Group (TSG), Radio Access Network (RAN), Working Group (WG4). *UE Radio Transmission and Reception (FDD)*. TS 25.101, V3.4.1, 2000.
- [2] 3rd Generation Partnership Project (3GPP), Technical Specification Group (TSG), Radio Access Network (RAN), Working Group (WG4). *Base Station Conformance Testing (FDD)*. TS 25.141, V3.3.0, 2000.
- [3] S. Affes, H. Hansen, and P. Mermelstein. Interference subspace rejection in wideband CDMA - part I: modes for mixed-power operation. *submitted to IEEE Journal on Selected Areas in Communications*, October 2000.
- [4] S. Affes, H. Hansen, and P. Mermelstein. Interference subspace rejection in wideband CDMA - modes for mixed-power operation. In *Proc. ICC'01*, volume 2, pages 523–529, 2001.
- [5] S. Affes and P. Mermelstein. A new receiver structure for asynchronous CDMA: STAR - the spatio-temporal array-receiver. *IEEE Journal on Selected Areas in Communications*, 16(8):1411–1422, October 1998.
- [6] K. Cheikhrouhou, S. Affes, and P. Mermelstein. Impact of synchronization on receiver performance in wideband CDMA networks. In *Proc. of 34th Asilomar Conference on Signals, Systems, and Computers*, pages 252–258, 2000.
- [7] K. Cheikhrouhou, S. Affes, and P. Mermelstein. Impact of synchronization on performance of enhanced array-receivers in wideband CDMA networks. *Accepted for publication in IEEE Journal on Selected Areas in Communications*, 4th Quarter 2001. to appear.
- [8] M. Landolsi and W. Stark. DS-SS-CDMA chip waveform design for minimal interference under bandwidth, phase, and envelope constraints. *IEEE Trans. on Communications*, 47(11):1737–1746, November 1999.
- [9] A. Naguib. *Adaptive Antennas for CDMA Wireless Networks*. Ph.D dissertation, Stanford University, Stanford, USA, 1996.
- [10] S. Parkvall. Variability of user performance in cellular DS-SS-CDMA - long versus short spreading sequences. *IEEE Trans. on Communications*, 48(7):1178–1187, July 2000.
- [11] J. Shynk. Frequency-domain and multirate adaptive filtering. *IEEE Signal Processing Magazine*, 9(1):14–37, January 1992.
- [12] B. Suard, A. Naguib, G. Xu, and A. Paulraj. Performance analysis of CDMA mobile communication systems using antenna arrays. In *Proc. ICASSP'93*, volume VI, pages 2421–2424, 1996.
- [13] J. Tugnait, L. Tong, and Z. Ding. Signal-user channel estimation and equalization. *IEEE Signal Processing Magazine*, 17(3):17–28, May 2000.
- [14] A. Viterbi. *CDMA Principles of Spread Spectrum Communication*. Addison-Wesley, 1995.
- [15] T. Wong, T. Lok, and J. Lehnert. Asynchronous multiple-access interference suppression and chip waveform selection with aperiodic random sequences. *IEEE Trans. on Communications*, 47(1):103–114, January 1999.